Turkish Journal of Electrical Engineering & Computer Sciences

http://journals.tubitak.gov.tr/elektrik/

Research Article

Turk J Elec Eng & Comp Sci
(2017) 25: 1894 – 1907

doi:10.3906/elk-1603-170

Optimum design and operation analysis of permanent magnet-assisted synchronous reluctance motor

Jamal DEHGHANI ASHKEZARI[1,*], Hassan KHAJEROSHANAEE[1], Mohsen NIASATI[2], Mohammad JAFAR MOJIBIAN[3]

[1]Young Researchers and Elite Club, Najafabad Branch, Islamic Azad University, Najafabad, Iran
[2]Department of Electrical & Computer Engineering, Faculty of Engineering, Semnan University, Semnan, Iran
[3]Department of Electrical & Computer Engineering, Faculty of Engineering, K.N. Toosi University of Technology, Tehran, Iran

Received: 15.03.2016 • **Accepted/Published Online:** 12.07.2016 • **Final Version:** 29.05.2017

Abstract: This paper presents an optimum design process and operational analysis of a permanent magnet-assisted synchronous reluctance motor (PMASynRM) as a low-cost and highly efficient consumed magnet material machine. The motor's topology is based on inserting partial permanent magnetic materials into flux barriers of an original synchronous reluctance motor (SynRM) that implicitly increase the difference between the machine's inductances, thereby increasing output torque. The procedure of rotor design as the main contribution of this paper is carefully illustrated. The rectangular shape of the flux barriers was found to achieve cost reduction and improve productivity. The impact of the permanent magnet added to the rectangular flux barriers and how it decreases the q-axis flux are described. For analytical studies, the optimum structure of a sample machine for high-power application is designed through the 2D finite element method in a Maxwell environment. For the sample machine, it is shown that the optimum number of flux barriers, optimum insulation ratio, and optimum width of permanent magnets in order to maintain the rating level of output and minimize the ripple are 4, 0.375, and 30 mm, respectively. In addition to demonstrating the operation of the motor with and without permanent magnet material, the performance of the hybrid motor is evaluated with two different permanent magnet materials, ferrite and NdFeB. Simulation results show that despite a negligible rise of ripple torque, the PMASynRM is able to achieve a higher output torque than the original SynRM with a low amount of permanent magnet material.

Key words: Electrical motor, permanent magnet-assisted synchronous reluctance motor, machine design, finite element method, Maxwell

1. Introduction

One of the primary objectives of different industries is to equip application devices with electrical ones, i.e. old and depreciated systems are replaced with electrical technology. The main required component of such an apparatus is an electrical motor or generator. Moreover, adaptation of existing electrical equipment in order to meet industrial needs can reduce costs and delay massive investments for any organization. A reasonable way for enhancing variables such as the output torque, operational speed range, and efficiency of electrical machines is the combination of two or more machines so that it not only preserves the advantages of them individually but also promotes them together.

*Correspondence: jda.ashk@gmail.com

There is a large body of scientific research that is related to synchronous magnetic and reluctance motors. Different structures are introduced and in some cases they are realized to the construction phase [1,2]. In particular, the more magnetic material specifications dramatically improve, the more magnetic motors are developed. Magnetic-type motors are divided into two categories: permanent magnet synchronous motors (PMSMs) and brushless DC (BLDC) motors. Magnetic-type motors have an appropriate performance at fundamental frequency; however, their operational speed range is narrow [3,4].

Reluctance-type motors have no magnetic material in their topology, which eliminates the demagnetization problem and consequently makes them suitable for working in high-temperature conditions. The main operation principle of reluctance-type motors is based on the difference in the q- and d-axis reluctances. Reluctance-type motors are classified as switched reluctance motors (SRMs) and synchronous reluctance motors (SynRMs). The SRMs have field coils as in a DC motor for the stator windings, while the rotor has no magnet or coils. SRMs are designed so that both the stator and rotor have salience poles and their numbers of poles are not usually the same. A SRM operates on reluctance torque and its speed is directly proportional to the pulse frequency of the input supplied. In spite of a high power density at low cost, which makes it ideal for many applications, one serious concern about SRMs is high torque ripple when they operate at low speed. SynRMs are low-cost and generate reluctance torque through the magnetic saliency of the rotor without any magnetic material. Unlike induction motors (IMs) that include stator copper loss as well as rotor copper loss, such loss is eliminated in SynRMs due to the magnet-free rotor. This means that SynRMs feature the same output from a smaller size or higher output from the same size as an IM. Moreover, for the same output, a SynRM can achieve higher efficiency than that of an IM because of lower loss caused by the magnet-free rotor. Thus, SynRMs are considered as high-efficiency motors and good substitutes for IMs. In comparison to a PMSM, SynRMs have more copper loss, which is why they have lower efficiency [5]. The reason for this is that, for the same output, the SynRM absorbs a higher current than the PMSM. In the other words, since the SynRM only outputs reluctance torque and there is no magnetic torque, for the same output as the PMSM, a higher current must be supplied to the SynRM. This additional current flowing through the stator results in more loss and thereby lower efficiency.

The permanent magnet-assisted synchronous reluctance motor (PMASynRM) was designed to provide the advantages of both the SynRM and PMSM. The PMASynRM can be evolved from a SynRM. The PMASynRM has attracted a lot of interest from researchers [6,7]. Due to the combinative nature of its structure, it generates both magnetic and reluctance torque. The magnetic and reluctance torques, depending on the type of flux barrier shape, can be generated by various topologies of the rotor. The flux barriers of the rotor can be either an arc or rectangular in shape. In [8], a suitable method for efficiency evaluation of a PMASynRM with magnetic nonlinearity and a rectangular flux barrier was proposed. A permanent magnet was only inserted into two sides of the rectangular flux barriers. The concentration was only on the efficiency and other properties such as the optimum value of the permanent magnet were not discussed. A PMASynRM with ferrite magnets for high-power applications was designed and its characteristics were compared with a rare-earth PMSM in [9]. The magnets were inserted into the entire flux barriers approximately, while no discussion about the optimum number of flux barriers or optimum amount of magnets was reported. Shohei et al. examined a PMASynRM with ferrite magnets and arc-shaped flux barriers to satisfy the mechanical strength requirements in the high-speed region [10]. The entire space of flux barriers contains magnets to provide an equal power speed range in comparison to a rare-earth PMSM. In [11], the impact of stack length on copper and iron loss of a PMASynRM and improvement of efficiency characteristics were investigated. An operating comparison between

a spoke-type PMSM and PMASynRM with ferrite magnets and arc-shaped flux barriers was also provided in [12]. Accordingly, the PMASynRM was unable to produce a higher torque density than that of the spoke-type PMSM. The authors in [13] claimed that a PMASynRM with ferrite magnets and arc-shaped flux barriers can be competitive against the PMSM for automotive applications. To this end, however, a large amount of magnets must be inserted into the flux barriers. A PMASynRM was designed with ferrite magnets and rectangular flux barriers considering productivity in [14]. It was shown that the rectangular shape of the flux barriers can achieve cost reduction and improve productivity [14].

In this paper, a scheme based on inserting a permanent magnet into the rotor of a SynRM is proposed. It changes the q-axis flux value so that the overall torque is improved [15]. A more detailed discussion of the strategy is included in the next sections. The rest of the paper is organized as follows: the influence of the added permanent magnet on the output torque equation is discussed in the next section. In Section 3, general design principles of the PMASynRM are provided. Optimum modeling of a sample machine obtained through equations and simulation results are presented in Section 4. Finally, concluding remarks are given in Section 5.

2. The impact of a permanent magnet added to a reluctance motor

The PMASynRM can be evolved by adding permanent magnet material to the flux barriers of a SynRM, as shown in Figure 1. The output torque equation of a SynRM caused by rotor saliency is as follows [5]:

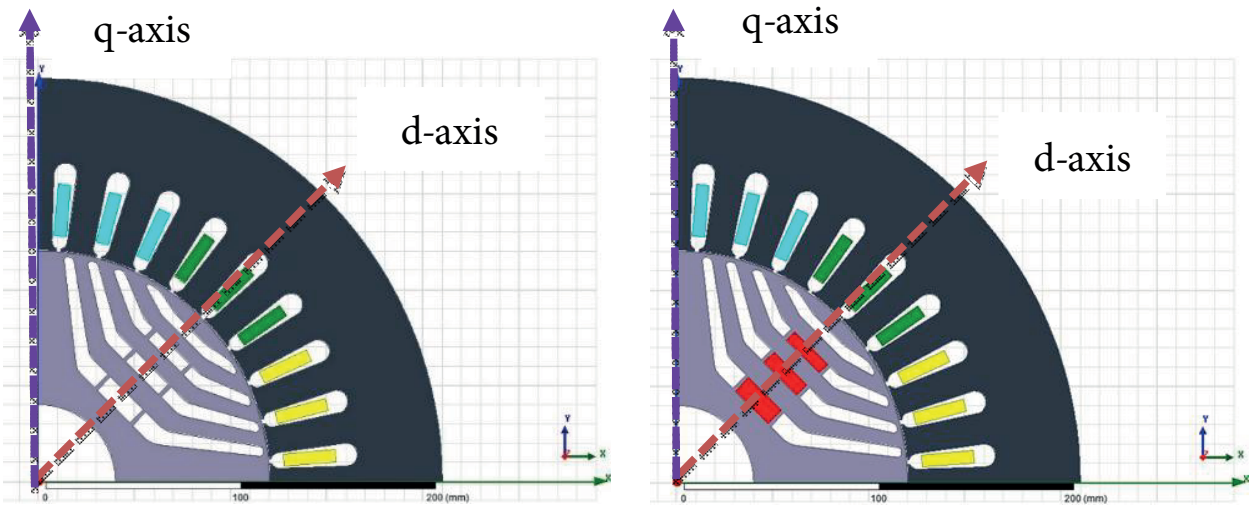

(a) (b)

Figure 1. Schematics of studied motors: a) original SynRM, b) PMASynRM.

$$T = P(L_d - L_q)i_d i_q = P\{(L_d i_d)iq - (L_q i_q)i_d\}, \tag{1}$$

where P is the number of pairs of poles, i_d is the d-axis current, i_q is the q-axis current, and L_d and L_q are the d- and q-axis inductance, respectively. The output torque is generated due to the difference in the q- and d-axis inductances of the machine. As can be seen from Eq. (1), there is a large negative component at the second term, which is responsible for increasing the motor current. The normal value of the negative component is about 0.2 p.u. for a typical SynRM [5]. The motor has to be designed so that it has low q-axis inductance as much as possible and so that the negative component can be reduced more. However, the q-axis inductance cannot be greatly reduced.

In a PMASynRM, the second term of Eq. (1) is reduced by adding permanent magnet material as an auxiliary part reducing the q-axis flux. The torque equation and phasor diagram of the PMASynRM are given in Eq. (2) and Figure 2, respectively. Here, φ_a is the linkage internal flux of the auxiliary permanent magnet material. As shown in Figure 2, the permanent magnet materials are placed in the flux barrier in such a way that its flux is the exact opposite of the flux corresponding to the q-axis. It is worth noting that the value of φ_a cannot be increased continuously. There is an optimum value of φ_a ($\varphi_{a,opt}$) such that, for higher values, the impact of the permanent magnet material is negative.

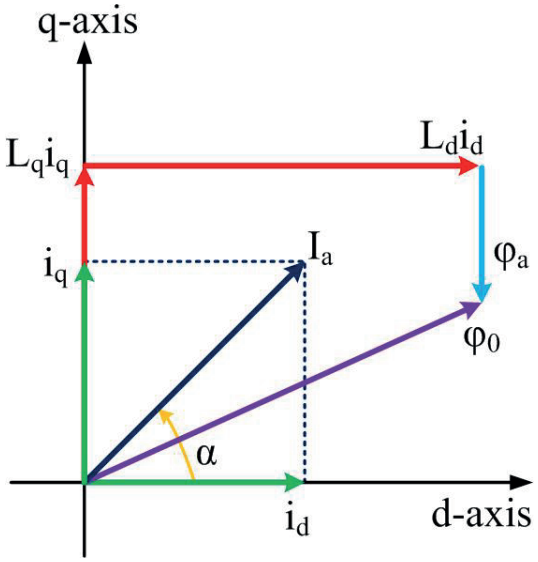

Figure 2. The q- and d-axis currents and the flux of a PMASynRM.

$$T = P\{(L_d i_d) iq - (\varphi_a - L_q i_q) i_d\} \tag{2}$$

3. The main principle of the PMASynRM design

The rotor schematic of a PMASynRM is depicted in Figure 1. Inside the rotor are a few slots that are known as flux barriers, into which the partial permanent magnet is inserted. The permanent magnets are uniformly magnetized and form the d-axis of the rotor. As the permanent magnets have approximately the same permeability as air, they create a path with high reluctance and magnetic anisotropy in the d-axis direction. The iron part of the rotor is formed from a smaller segment, isolated from each other by the flux barriers. These iron parts provide a low reluctance path for the q-axis flux. For considering stability problems, it is necessary that iron segments be internally connected together, so tangential ribs close to the air gap are used in the rotor structure. Due to inserting the permanent magnets, the tangential ribs are saturated during normal operation of the motor and therefore they magnetically isolate various iron segments. From the viewpoint of torque production, leakage flux caused by tangential ribs must be as low as possible. Due to mechanical power restrictions, however, the minimum width of tangential ribs must not be set to less than 1 mm [16].

It is interesting to introduce some geometrical parameters of the rotor. In Figure 3, a rotor of a PMASynRM with four flux barriers (B1, B2, B3, and B4) is represented where T_m is the thickness of slots along the d-axis. Thus, T_s is the thickness of the iron segments along the d-axis. W_m and W_b are the length of the

flux barriers in the direction perpendicular to the d-axis and the direction parallel to the q-axis, respectively. The thickness of the flux barriers along the q-axis is shown by T_b. The endpoint angle of the flux barrier is indicated by α_m, which can be calculated through Eq. (3a), where p is the number of poles, k is the number of flux barriers, and α_e is the end-point angle of the flux barrier in electrical degrees. Considering a constant rotor slot pitch, then:

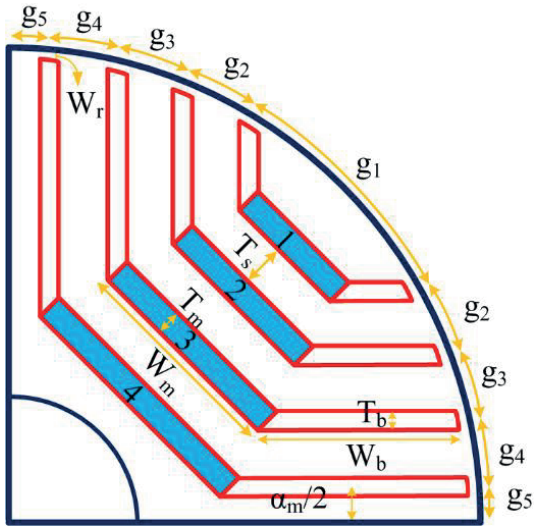

Figure 3. Rotor cross-section of a PMASynRM.

$$\alpha_m = \frac{\frac{\pi}{p}}{k+1}, \tag{3a}$$

$$\alpha_e = \frac{p}{2}\alpha_m. \tag{3b}$$

A useful parameter known as the isolation ratio for comparing the dimensions of the flux barriers is expressed as follows:

$$K_w = \frac{w_{ins}}{w_{iron}}, \tag{4}$$

where W_{ins} and W_{iron} are the total width of the flux barriers and iron segments, respectively. K_{wd} denotes the insulation ratio along the d-axis while K_{wq} refers to that of the q-axis. Normal values of the insulation ratio for the d- and q-axis can be assumed as 0.6 and 0.3, respectively [18]. A detailed study of the impact of insulation ratio variation is illustrated in the following. For a given insulation ratio K_{wd}, the total thickness of iron segments along the d-axis can be obtained as follows:

$$T_{sd} = \frac{D/2 - D_{rc}/2}{1 + K_{wd}}, \tag{5}$$

where D and D_{rc} refer to the outer diameter of the rotor and the shaft diameter, respectively. In order to determine the relative thickness of the each iron segment, it is assumed that magnetomotive force (MMF) is sinusoidally distributed, there is no leakage flux, and the entire flux caused by the MMF is shared between

related parts. The thickness of each iron segment is specified using Eq. (6), which is taken from [17,18]:

$$\frac{T_{si}}{T_{si+1}} = \frac{\sin[\alpha_e(2i-0.5)] - \sin[\alpha_e(2i-1.5)]}{\sin[\alpha_e(2i+1.5)] - \sin[\alpha_e(2i-0.5)]}, i = 1, 2, 3, ..., k. \tag{6}$$

The total thickness of the flux barriers along the d-axis is calculated as follows:

$$T_{md} = \frac{D/2 - D_{rc}/2}{1 + 1/K_{wd}}. \tag{7}$$

To determine the relative thickness of the flux barriers, it is assumed that the permeability ratio of the flux barriers is constant. This leads to sinusoidal distribution of the flux density in the air gap and thus a smoother waveform of torque. The relative thickness of the flux barriers is obtained from the equations below [17,18]:

$$\frac{T_{m,i+1}}{T_{m,i}} = (\frac{num}{denum})^2, i = 1, 2, 3, ..., k-1, \tag{8a}$$

$$num = \sin[\alpha_e(2i+3.5)] - \sin[\alpha_e(2i+2.5)] - \sin[\alpha_e(2i+1.5)] + \sin[\alpha_e(2i+0.5)], \tag{8b}$$

$$denum = \sin[\alpha_e(2i+1.5)] - \sin[\alpha_e(2i+0.5)] - \sin[\alpha_e(2i-0.5)] + \sin[\alpha_e(2i-1.5)]. \tag{8c}$$

For a given isolation ratio K_{wd}, Eq. (8a) can be used to determine the flux barriers. The total available thickness along the q-axis to work out the flux barriers and iron segment can be calculated as follows:

$$l_q = (\frac{D}{2})\sin(\frac{\pi}{p}), \tag{9}$$

where l_q is the total available thickness along the q-axis. It should be noted that the total iron value along the q-axis must be equal to or larger than that along the d-axis to ensure greater q-axis inductance. Similar to the approach applied to the d-axis, the total thickness of flux barriers along the q-axis (T_{bq}) can be obtained by subtraction of the total iron value from the total available length of the q-axis, i.e. l_q. The value of the insulation ratio along the q-axis is different from that of the d-axis, which can be calculated as follows:

$$K_{wq} = \frac{T_{bq}}{l_q - T_{bq}}. \tag{10}$$

The relative thickness of flux barriers along the q-axis can be obtained by following a procedure similar to that provided for the d-axis.

4. Optimum value calculation for the rotor

The above-mentioned design principles are examined considering a typical sample machine. The primary specification of the machine is provided in Table 1. First, the design procedure is performed using the theoretical equations stated in previous sections. Then a model of the rotor is synthesized using the analytical results and it is simulated in a Maxwell environment in order to obtain a complementary analysis of the model. In the following, selection of parameters as well as corresponding simulations of various conditions are discussed.

Table 1. The primary data of the sample machine.

Parameter (unit)	Value
Number of phases	3
Rated voltage (V)	560
Frequency (Hz)	133
Rated speed (rpm)	4000
Rated torque (Nm)	716
Number of slots	36
Outer diameter of stator (mm)	420
Total axial length (mm)	325
Outer diameter of rotor (mm)	240
Shaft diameter (mm)	80
Air gap height (mm)	0.6
Tangential ribs thickness (mm)	2
Rated current (peak/rms) (A)	608/430

4.1. Number of flux barriers

This section deals with selecting the most appropriate number of flux barriers for the machine under study. To this end, under fixed conditions for all parameters, only the number of flux barriers varies from 1 to 7 so that the insulation ratio remains constant. The schematics of a rotor with 1 and 7 flux barriers are represented in Figures 4a and 4b, respectively. In order to determine the proper number of flux barriers, two criteria are considered and compared for all cases: the average output torque and the ripple value of output torque, their curves being given in Figures 5 and 6, respectively. Figure 5 provides average output torque corresponding to all considered cases, including 1 flux barrier up to 7 flux barriers. Referring to Figure 5, it can be concluded that with up to 4 flux barriers, the average output torque increases linearly. For numbers of flux barriers higher than 4, the average output torque is already constant, while it imposes mechanical problems on the design procedure. This agrees with what was outlined in [18] about the number of flux barriers. We can also see from Figure 6 that the minimal value of ripple torque is obtained for 4 flux barriers. Therefore, increasing the number of flux barriers above 4 is not justifiable, neither for average output torque nor the ripple value of output torque.

4.2. Insulation ratio

To determine the optimum total thickness of flux barriers (or the optimum insulation ratio) for achieving maximum output torque, the performance of the PMASynRM is investigated by varying the thickness of flux barriers. Here, the optimum insulation ratio is obtained for two different cases. First, under fixed conditions for all parameters, only the insulation ratio along the d-axis (K_{wd}) is changed by varying the thickness of the flux barrier while it is assumed that the rotor has a single flux barrier. Considering the average output torque, the optimum thickness of the flux barrier and the corresponding insulation ratio for a single flux barrier are obtained as 40 mm and 0.5, respectively, as shown in Figure 7. If the optimum insulation ratio remains constant for any rotor topology with a different number of flux barriers, then for optimum total thickness of a single flux barrier and knowing the optimum number of flux barriers obtained from the previous section (i.e. 4), the thickness of each flux barrier can be calculated using Eqs. (8a) to (8c).

As the optimum insulation ratio is not essentially identical for rotors with different numbers of flux barriers, under fixed conditions for all parameters and in the case of 4 flux barriers, we only vary the insulation

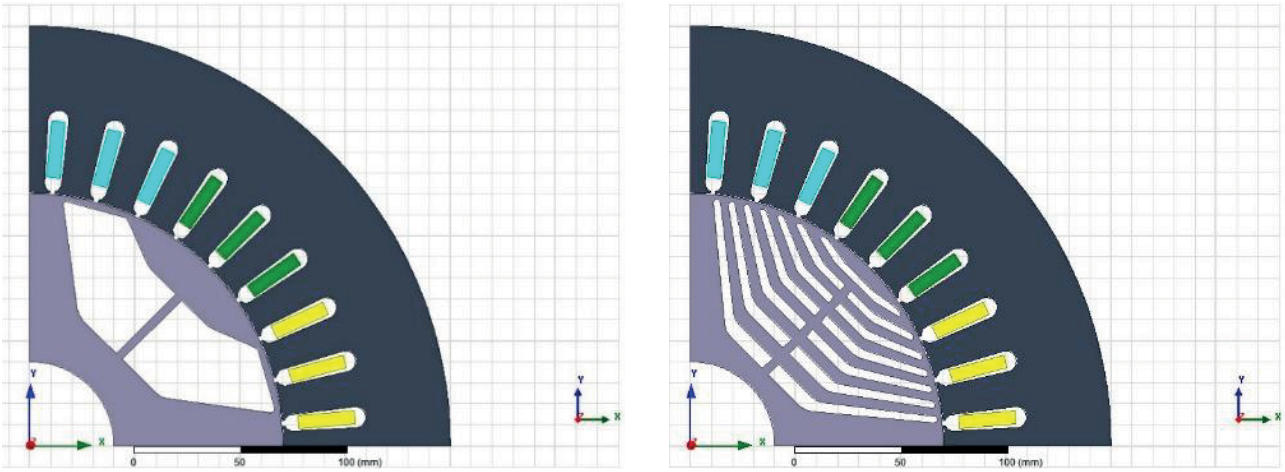

(a) (b)

Figure 4. Schematics of the studied rotors: a) 1 flux barrier and b) 7 flux barriers.

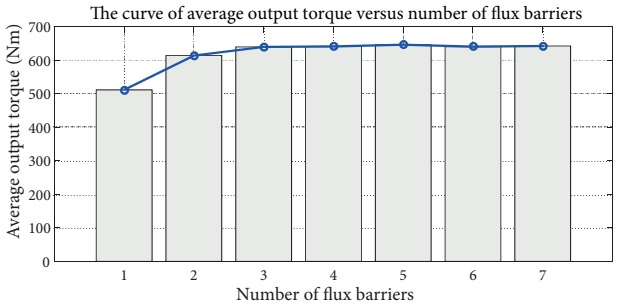

Figure 5. Average output torque of a PMASynRM for varying numbers of flux barriers.

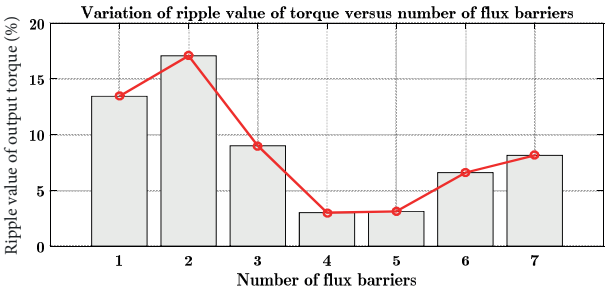

Figure 6. Ripple value of output torque of a PMASynRM for varying numbers of flux barriers.

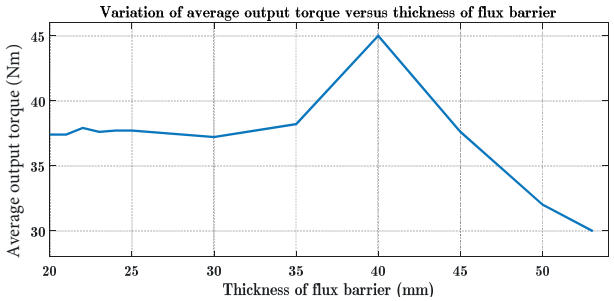

Figure 7. Average output torque of a PMASynRM with a single flux barrier for varying thicknesses of flux barriers.

ratio (K_{wd}) by variation of the thickness of the 4th flux barrier (B4) from 6 mm up to 14 mm by steps of 2 mm, and for each state, the thicknesses of other flux barriers are obtained using Eqs. (8a) to (8c). The schematics of the rotor and corresponding thicknesses of flux barriers are given in Figure 8. The average and ripple values of output torque are monitored continuously, as shown in Figure 9 (the ripple value is scaled by a factor of 10 such that its magnitude is comparable to that of the average torque). It can be seen that the optimum thickness of the 4th flux barrier is 10 mm, resulting in the minimum ripple and the maximum average torque. Under

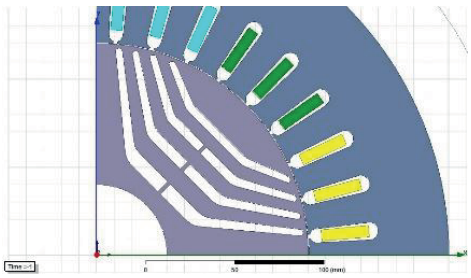

a) Kwd = 0.23

	B4	B3	B2	B1	T_{md}
Thick. (mm)	6.00	4.75	4.05	3.60	18.40

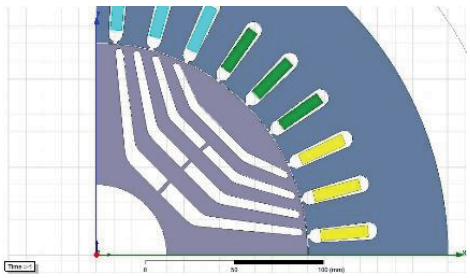

b) Kwd = 0.30

	B4	B3	B2	B1	Tmd
Tick. (mm)	8.00	6.22	5.27	4.66	24.15

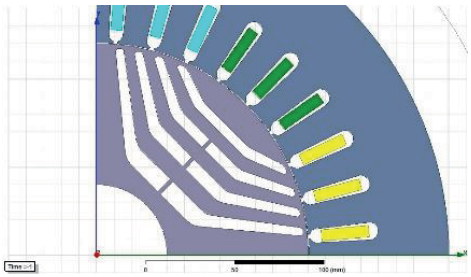

c) K_{wd} = 0.375

	B4	B3	B2	B1	Tmd
Thick. (mm)	10.00	7.70	6.60	5.70	30.00

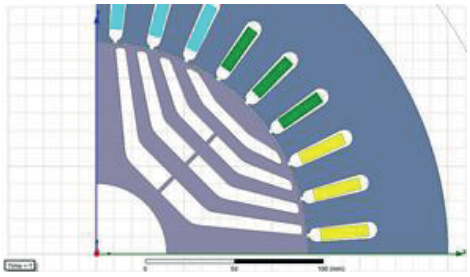

d) Kwd = 0.44

	B4	B3	B2	B1	Tmd
Thick. (mm)	12.00	9.03	7.57	6.66	35.26

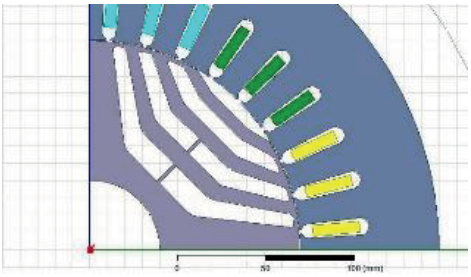

e) Kwd = -

	B4	B3	B2	B1	Tmd
Thick. (mm)	14.00	10.39	8.67	Open end	-

Figure 8. The thickness variation of flux barriers to obtain an optimum insulation ratio: a) B4 = 6 mm, b) B4 = 8 mm, c) B4 = 10 mm, d) B4 = 12 mm, e) B4 = 14 mm.

such circumstances, the thickness of the 3rd, 2nd, and 1st flux barrier is 7.70 mm, 6.60 mm, and 5.70 mm, respectively, and the total thickness of flux barriers along the d-axis becomes 30 mm ($T_{md} = 30$ mm). The corresponding insulation ratio along the d-axis for $T_{md} = 30$ mm is also 0.375. Thus, the optimum insulation ratio for rotors with various flux barriers is not the same, and it must be separately obtained for each case. For the sample machine, it was found that the optimum number of flux barriers is 4 and the corresponding optimum insulation ratio is 0.375.

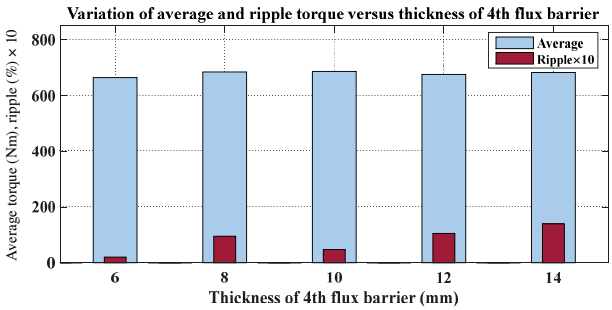

Figure 9. Average and ripple output torque of a PMASynRM with 4 flux barriers for varying insulation ratios.

4.3. Permanent magnet width

The width of the permanent magnet material has a tangible impact on the output torque of the motor. For investigation of the effect of permanent magnet size on the output torque, knowing the exact number of flux barriers and their thickness (4 and 0.375, respectively), we now calculate the optimum amount of magnet for each flux barrier. The length of each magnet is equal to the length of the corresponding flux barriers into which it was inserted. Three different cases of NdFeB magnets with widths of 15 mm, 25 mm, and 40 mm were evaluated to draw the curve. Figure 10 shows the three different topologies. The curve of average output torque and the ripple value of output torque corresponding to variation of permanent magnet width are depicted in Figures 11 and 12, respectively. For the given machine and in order to satisfy the rating output requirement, it is sufficient to insert magnets into flux barriers 2, 3, and 4. Adding the magnet to flux barrier 1 will not remarkably improve the average output torque while it results in increasing ripple value. It is possible that for another machine it would be necessary to insert a magnet into all four flux barriers. In the case of magnets inserted into flux barriers 2, 3, and 4 and as long as the width of the permanent magnet increases up to 30 mm, the average output torque increases, too, while the behavior of ripple output torque is nonlinear, i.e. up to 15 mm it has a modest rise to about 5.15% and then up to 30 mm it has a low decline and reaches about 4.8%. Over the higher values of permanent magnet width, the average output torque is approximately constant while the ripple torque is increased. Therefore, according to this information, the optimum value of permanent magnet width is 30 mm for flux barriers 2, 3, and 4.

4.4. Investigation of role and type of permanent magnet

Finally, after optimum designing of different parts of the machine, it is desirable to compare it with the original SynRM. For this purpose, the original SynRM with two different types of rectangular flux barriers and the optimum designed PMASynRM shown in Figure 13 are compared from viewpoints of average and ripple value of the output torque. The obtained results are given in Table 2. It can be observed that the PMASynRM is able to enhance average output torque by about 10% with a slight rise in ripple value. As the rating output is high, improvement by 10% is a considerable increase of output torque. Moreover, similar to what was done in

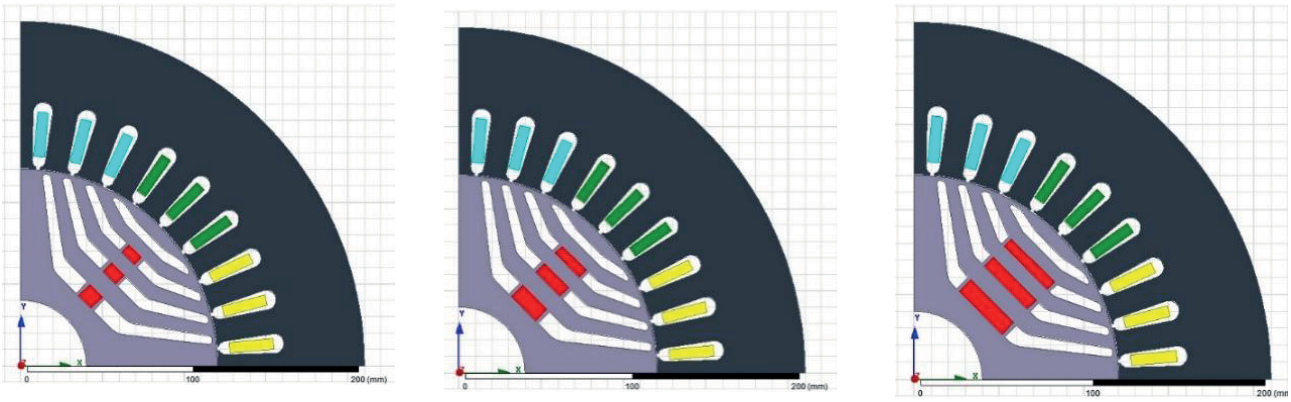

(a) (b) (c)

Figure 10. Rotor topologies with different widths of permanent magnet: a) 15 mm, b) 25 mm, and c) 40 mm.

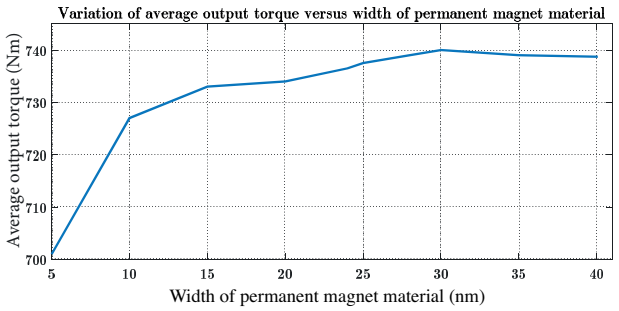

Figure 11. Average output torque of a PMASynRM for varying widths of permanent magnets inserted into B4, B3, and B2.

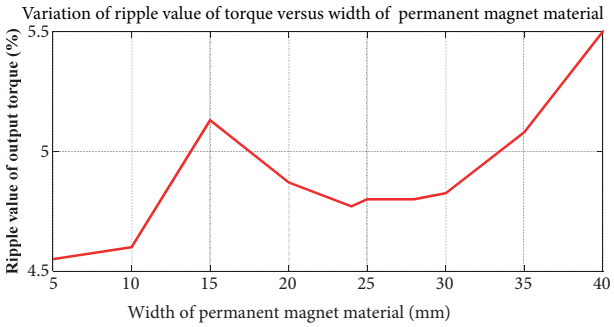

Figure 12. Ripple value of output torque of a PMASynRM for varying widths of permanent magnets inserted into B4, B3, and B2.

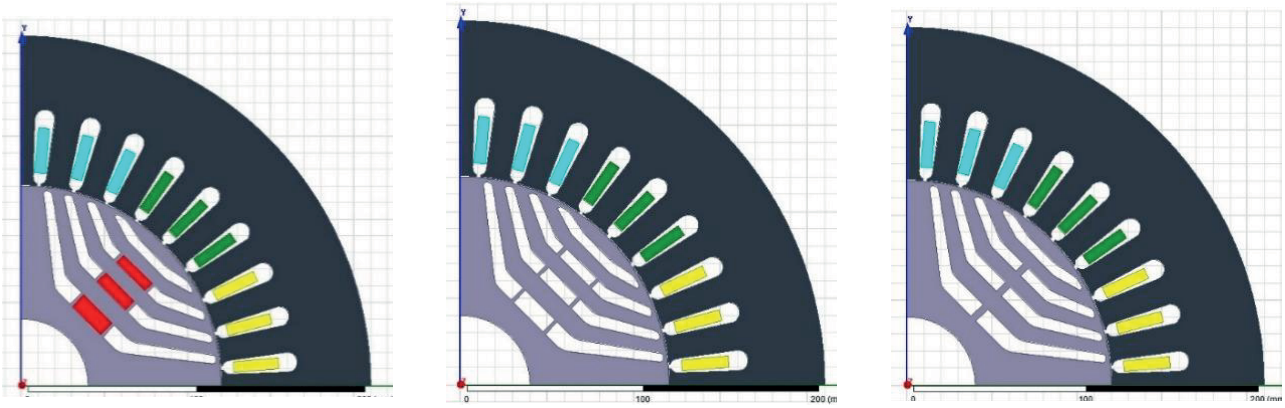

(a) (b) (c)

Figure 13. Three topologies with and without permanent magnet: a) with permanent magnet; b) without permanent magnet, case 1; c) without permanent magnet, case 2.

[18], the direct impact of the permanent magnet type is investigated using two different permanent magnets, ferrite and NdFeB. In the PMASynRM only a small amount of permanent magnet is used. Ferrite has a much

lower residual flux density (Br) than NdFeB. However, it remarkably lowers the cost of the motor in comparison to NdFeB and increases the power factor and efficiency. On the other hand, the permanent magnet must satisfy the requirement of machine torque. The impacts of the permanent magnet type on the average output torque and its ripple value with both ferrite and NdFeB are evaluated. It is assumed that the residual flux density (Br) and magnetic field intensity (H) for full demagnetizing of the NdFeB are 1.2 T and 965 kA/m, respectively, while corresponding values for ferrite are 0.4 T and 195 kA/m, respectively. The average output torque and its ripple value considering two different materials are reported in Table 3. It can be clearly seen from Table 3 that significant different values for the average produced torque are obtained, i.e. the corresponding values for ferrite are less than those for NdFeB. In the other words, for the same required output torque, a greater amount of ferrite is needed than that of NdFeB. In particular, for a high-power application such as a submarine drive system, it is possible that ferrite cannot satisfy the required conditions. In addition, there is a great increase for the ripple value of output torque when ferrite is used. These considerations must be taken into account for realizing an appropriate machine.

Table 2. Average output torque and ripple value of designed PMASynRM with and without permanent magnet material.

	Ripple value (%)	Average output torque (Nm)
With permanent magnet	3.75	734
Without permanent magnet, case 1	3.02	674
Without permanent magnet, case 2	2.66	668

Table 3. Average output torque and ripple value of PMASynRM for two different permanent magnet material.

	Ripple value (%)	Average output torque (Nm)
Ferrite	12.9	435
NdFeB	3.75	734

5. Conclusion

The design procedure of a PMASynRM evolved from a SynRM was investigated. The impact of inserting permanent magnet material into flux barriers of the SynRM was discussed. It was clear that the permanent magnet material increases the difference between the machine's inductances and results in the increasing of output torque. The design principles of the rotor for a PMASynRM were provided in more detail. Moreover, the optimum values for a given sample machine were obtained through simulation results. The most important outcomes can be summarized as follows:

- The impact of the permanent magnet material is the change of saliency ratio and inductances so that it improves the output torque.
- A PMASynRM can simultaneously provide the advantages of both the SynRM and PMSM.
- Increasing the number of flux barriers up to 4 improves the average output torque and decreases the ripple value. For a higher number of flux barriers, there is not a significant increase in the output torque.
- The average output torque is directly affected by the insulation ratio. There is an optimum insulation ratio that results in the maximum average output torque. Furthermore, the optimum insulation ratio for a given machine and under different numbers of flux barriers is not essentially the same. In the sample

machine in this study, the optimum design insulation ratio for one and for four flux barriers was 0.5 and 0.375, respectively.

- The behavior of the ripple value considering the volume of used permanent magnet material is nonlinear and there is an optimum value in order to maintain the rating level of average output torque and to achieve the minimum ripple value. For the sample machine in this study, the width of permanent magnets was found to be 30 mm when they were only inserted into B2, B3, and B4.

- For the final design of the given machine, inserting the permanent magnet into flux barriers increased the average output torque by 10% and slightly increased the ripple value in comparison to cases without permanent magnet material.

- The performance of the machine with NdFeB is better than that with ferrite. However, using a ferrite permanent magnet achieves a low-cost machine. Proper selection of the permanent magnet should be taken into account considering the application of the PMASynRM. It was found that for the same output value, a larger amount of ferrite is needed in comparison to NdFeB.

References

[1] Vartanian R, Toliyat H. Design and comparison of an optimized permanent magnet-assisted synchronous reluctance motor (PMa-SynRM) with an induction motor with identical NEMA frame stators. In: IEEE 2009 Electric Ship Technologies Symposium; 20–22 April 2009; Baltimore, MD, USA. New York, NY, USA: IEEE. pp. 107-112.

[2] Betz RE. Control of synchronous reluctance machines. In: IEEE 1991 Industry Applications Conference; 28 September–4 October 1991; Dearborn, MI, USA. New York, NY, USA: IEEE. pp. 456-462.

[3] Chalmers BJ, Musaba L, Gosden DF. Variable-frequency synchronous motor drives for electrical drives. IEEE T Ind Appl 1996; 32: 896-903.

[4] Chalmers BJ, Akmese R, Musaba L. Design and field weakening performance of permanent-magnet/reluctance motor with two-part rotor. IEE P-Elect Pow Appl 1998; 145: 133-139.

[5] Murakami H, Honda Y, Sadanaga Y, Ikkai Y, Morimoto S, Takeda, Y. Optimum design of highly efficient magnet assisted reluctance motor. In: IEEE 2001 Industry Applications Conference; 30 September–4 October; Chicago, IL, USA. New York, NY, USA: IEEE. pp. 2296-2301.

[6] Guo W, Zhao Z, Zhang Y. Analysis and experimental study of slot effect in synchronous reluctance permanent magnet motors. In: IEEE 2006 International Power Electronics and Motion Control Conference; 13–16 August 2006; Shanghai, China. New York, NY, USA: IEEE. pp 1-6.

[7] Guo W, Zhao Z. Design and experiments of two glued axially laminated synchronous reluctance permanent magnetic motors. In: IEEE 2005 International Conference on Power Electronics and Drive Systems; 28 November–1 December 2005; Kuala Lumpur, Malaysia. New York, NY, USA: IEEE. pp. 1374-1379.

[8] Lee JH, Lee IK. Efficiency evaluation of PMASynRM versus SynRM using a coupled finite element method and Preisach modeling. Journal of Magnetics 2010; 15: 85-90.

[9] Obata M, Morimoto S, Sanada M, Inoue Y. Characteristic of PMASynRM with ferrite magnets for EV/HEV applications. In: IEEE 2012 International Conference Electrical Machines and Systems; 21–24 October 2012; Sapporo, Japan. New York, NY, USA: IEEE. pp. 1-6.

[10] Ooi S, Morimoto S, Sanada M, Inoue Y. Performance evaluation of a high-power-density PMASynRM with ferrite magnets. IEEE T Ind Appl 2013; 49: 1308-1315.

[11] Obata M, Shigeo M, Sanada M, Inoue Y. High-performance PMASynRM with ferrite magnet for EV/HEV applications. In: IEEE 2013 European Conference on Power Electronics and Applications; 3–5 September 2013; Lille, France. New York, NY, USA: IEEE. pp. 1-9.

[12] Montalvo-Ortiz EE, Foster SN, Cintron-Rivera JG, Strangas EG. Comparison between a spoke-type PMSM and a PMASynRM using ferrite magnets. In: IEEE 2013 Electric Machines & Drives Conference; 12–15 May 2015; Chicago, IL, USA. New York, NY, USA: IEEE. pp. 1080-1087.

[13] Morimoto S, Ooi S, Inoue Y, Sanada M. Experimental evaluation of a rare-earth-free PMASynRM with ferrite magnets for automotive applications. IEEE T Ind Electron 2014; 61: 5749-5756.

[14] Obata M, Morimoto S, Sanada M, Inoue Y. Performance of PMASynRM with ferrite magnets for EV/HEV applications considering productivity. IEEE T Ind Appl 2014; 50: 2427-2435.

[15] Morimoto S, Takeda Y. Permanent magnet assisted synchronous reluctance motor for wide constant power operation. In: IEEE 2000 Proceedings of International Power Electronics Conference; 3–7 April 2000; Tokyo, Japan. New York, NY, USA: IEEE. pp. 621-626.

[16] Khan KS. Design of a permanent-magnet assisted synchronous reluctance machine for a plug-in hybrid electric vehicle. Licentiate thesis, Royal Institute of Technology, Stockholm, Sweden, 2011.

[17] Rajabi R. Synchronous reluctance machine design. MSc, Royal Institute of Technology, Stockholm, Sweden, 2007.

[18] Lipo T, Miller T, Vagati A, Boldea I, Malesani L, Fukao T. Synchronous reluctance drives. In: IEEE 1994 Industry Applications Conference; 4–5 May 1994; Greenville, SC, USA. New York, NY, USA: IEEE.